J Fluoresc (2013) 23:407–415
DOI 10.1007/s10895-013-1155-4

ORIGINAL PAPER

Structural Characteristic of Folding/Unfolding Intermediate of Pokeweed Anti-viral Protein Revealed by Time-resolved Fluorescence

Shuzo Matsumoto · Yuka Taniguchi · Yukihiro Fukunaga · Hiromichi Nakashima · Keiichi Watanabe · Shoji Yamashita · Etsuko Nishimoto

Received: 14 September 2012 / Accepted: 7 January 2013 / Published online: 15 January 2013

Abstract The structural feature of unfolding intermediate of pokeweed anti-viral protein (PAP) was characterized using time-resolved fluorescence spectroscopic methods to elucidate protein folding/unfolding process. CD and fluorescence spectra consistently demonstrated that the unfolding of PAP completed at 4 M of guanidine hydrochloride (GuHCl). The fluorescence resonance energy transfer (FRET) and time-resolve fluorescence depolarization analysis of Trp208 and Trp237 located in the C-terminal domain of PAP suggested that peculiar unfolding intermediate populated before reaching to the unfolding state. The FRET distance of Trp237 to Tyr182 was extended to more than 28 Å with keeping the compact conformation in the unfolding intermediate state populated in the presence of 2 M GuHCl. On the other hand, Trp208 maintained the energy transfer pair with Tyr72 near the active site, although the rotational freedom was increased a little. There results suggest that the most distinguished structural feature of the unfolding intermediate of PAP is the separation of C-terminal domain from N-terminal domain. FRET and fluorescence depolarization studies also showed that C-terminal domain would be more separated to liberate the segmental motions of Trp208 and Trp237 distinctly at the unfolding state.

Keywords Protein folding/unfolding · FRET · Fluorescence depolarization · Ribosome-inactivating protein · Pokeweed anti-viral protein

Abbreviations

PAP	Pokeweed anti-viral protein
GuHCl	Guanidine hydrochloride
RIP	Ribosome-inactivating protein
FRET	Fluorescence resonance energy transfer
TCSPC	Time-correlated single photon counting

Introduction

The fluorescence spectroscopy is one of the most powerful methods to study the protein structure, function and dynamics by the progresses of excitation source, detection and analyzing system. The spectroscopic sensitivity is now so high that fluorescence photon emitted from even single molecule could be detected and the time-resolution power reached to several pico-seconds. When these advantages of the fluorescence spectroscopy is connected with specific photo-physical properties of tryptophan, interesting function-relating conformation and dynamics of protein can be investigated in detail through the unique analytical method such as fluorescence spectrum, resonance energy transfer, and depolarization. While the fluorescence spectroscopy is now widely used in

S. Matsumoto
Industrial Technology Center of Nagasaki, 2-1303-8, Ikeda, Ohmura, Nagasaki 856-0026, Japan

Y. Taniguchi · H. Nakashima · S. Yamashita · E. Nishimoto (✉)
Institute of Biophysics, Faculty of Agriculture, Graduate School of Kyushu University, Hakozaki, Fukuoka 812-8581, Japan
e-mail: enish@brs.kyushu-u.ac.jp

Y. Fukunaga
Institute for Material Chemistry and Engineering, Kyushu University, Kasuga, Fukuoka 816-8580, Japan

K. Watanabe
Department of Applied Biological Sciences, Saga University, Honjo, Saga 840-8502, Japan

biochemistry and molecular biology, one of the great achievements was recognized in the protein folding/unfolding studies [1]. The protein folding/unfolding process and mechanism is a central subject in protein sciences and is associated with many biological roles of protein. The gross and fundamental concept of protein folding has been elucidated through some potent protein folding models such as landscape, frame work and nucleation-condensation model [2-4]. Every these models demonstrate that nascent polypeptide would be folded to build 3D structure of protein through peculiar intermediate states. Therefore, specification of structure and pysico-chemical properties of the intermediate is an important clue to establish the protein folding/unfolding process and mechanism. The fluorescence spectroscopy can provide essential information to characterize the structural feature of the folding/unfolding intermediate.

An anti-viral protein from pokeweed (*Phytolacca americana*) (PAP) is a N-glycosidase (EC3.2.2.22) and catalyzes the adenine releasing reaction from ribosomal RNA. Because of this specific enzymatic action, PAP is classified as one species of ribosomal inactivating proteins (RIPs) included in almost every herbaceous plants [5-8]. Active site of PAP is constituted of two tyrosine, glutamate, and arginine residues. Tryptophan residue is arranged at the lid position of the active site to regulate the enzymatic activity [9]. Such specific structure near the active site is conserved in many RIPs and makes RIPs attractive protein for studying the protein folding/unfolding through the fluorescence spectroscopy, because the local structure near the active site of enzyme considered to be particularly folded and the detailed information would be obtained by the fluorescence spectroscopic properties of the tryptophan residue locate adjacently to the active site. Noting such specific arrangement of tryptophan residue of RIPs and the advantage of the fluorescence spectroscopy, Fukunaga et al. showed that one of RIPs, momorcharin prepared from seeds of bitter gourd, unfolded through a specific intermediate [10, 11]. According to them, the unfolding intermediate of α-momorcharin adopted more tightly packed structure than the folded state whereas the other β-momorcharin exhibited very similar properties with the ordinal molten globule (MG) state. It is quite interesting that each momorcharin unfolds through individual specific intermediate state in spite of the high homology in the amino acid sequence. The information obtained by the fluorescence studies of RIPs contribute to elucidation of the unresolved protein folding/unfolding mechanism.

In the present study, folding/unfolding of PAP was investigated because of the structural similarity with momorcharin and other RIPs. X-ray crystallographic structure shown in Fig. 1 reveals that PAP is constituted of N-terminal and C-terminal domains if they are assigned as the densely packed domain including 7 α-helices and 4 β-sheets, and the domain with hairpin and one α-helix, respectively. One of two

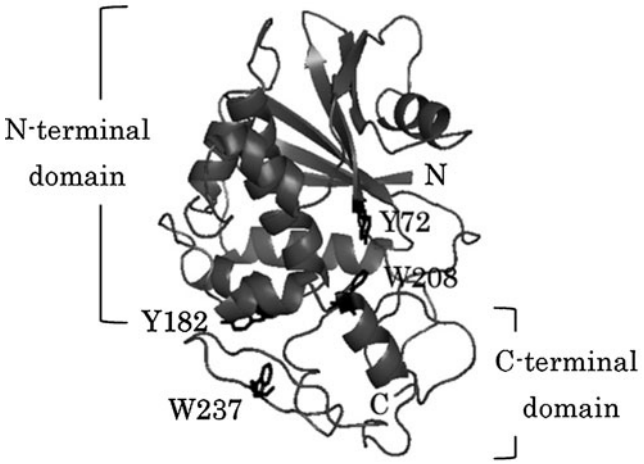

Fig. 1 The Crystal Structure of Pokeweed Anti-viral Protein (PAP). The crystal structure of PAP was presented (PDB accession code: 1PAF). N- and C-terminal positions are indicated by N and C. Two tryptophan residues in PAP, Trp208 and Trp237 and nearest neighboring Tyr72 and Tyr182 were indicated by *thick line*. The X-ray structure was drawn by PyMOL viewer

Trp residues, Trp237 is arranged in the C-terminal domain and the other, Trp208 takes a location of α-helix in C-terminal domain. Trp237 is adjacent to the N-terminal domain and Trp208 locate near the active site. Interestingly, two tyrosine residues, Tyr72 and Tyr182 which locate in the N-terminal domain adjoin Trp208 and Trp237, respectively. Such a specific arrangement of Tyr and Trp enables the application of fluorescence resonance energy transfer (FRET) analysis between them. In the present study, two mutant PAPs were prepared in order to investigate the topographical structure of the unfolding intermediate which populates in the process of denaturant-induced unfolding. One was W208F-PAP and the other W237F-PAP of which Trp208 and Trp237 were replaced with Phe, respectively. FRET between Trp and Tyr and molecular dynamic parameter obtained from the time-resolved fluorescence depolarization well depicted the characteristic features of the unfolding intermediate of PAP.

Materials and Methods

Materials

*Eco*RI and *Bam*HI were purchased from Nippon Gene Co Ltd. (Tokyo, Japan) and New England Biolabs Inc. (Ipswich, MA), respectively. DNA polymerase, KOD-plus-Ver. 2 was a product of Toyobo (Osaka, Japan). Tryptone and yeast extract were purchased from. Difco Laboratories (BD, Franklin Lakes, NJ). Factor Xa and Amylose resin for affinity column were purchased from Novagen (Merck KGaA, Darmstadt, Germany) and New England BioLabs Inc., respectively.

Mono S 5/50 GL was obtained from GE Healthcare UK (Buckinghamshire, UK) and used for cation exchange column chromatography.

Expression and Purification of Recombinant PAP

The expression of PAP was performed as described previously [12], except that the expression vector pMALY-p2 was used instead of pMAL-p2 (New England BioLabs). The pMALY-p2 yeast/Escherichia coli shuttle vector was constructed by inserting a 2 μ yeast replication origin and a URA3 selectable marker into pMAL-p2 as previously reported [13] and used for cloning and site-directed mutagenesis by in vivo homologous recombination in yeast [13, 14]. The DNA fragment encoding the mature region of PAP or its mutant was inserted between *Bam*HI and *Hind*III sites of pMALY-p2 and introduced into the *E. coli* strain XL1-Blue (Stratagene). The transformant was grown at 37 °C in 1 l of LB medium containing ampicillin (100 μg/ml) and tetracycline (12 μg/ml) to an OD of 1.0 at 600 nm, and then incubated with 0.35 mM isopropyl-β-D-thiogalactopyranoside for 5 h at 25 °C to induce expression of the PAP fusion with maltose-binding protein (MBP-PAP). The MBP-PAP was extracted from periplasmic fractions of harvested bacterial cells into distilled water including 5 mM $MgSO_4$ in the ice bath. After removing the debris by centrifugation, the sample solution was adopted to amylose resin affinity column to separate PAP from other protein. The maltose binding protein was removed using Factor Xa in 50 mM Tri-HCl buffer (pH8.0) including 0.1 M NaCl, 1 mM dithiothreitol and 5 mM $CaCl_2$. Wild type and mutant PAP were finally purified by Mono-S column using NaCl gradient from 0 to 0.3 M. Every chromatography was performed on Biologic DuoFlow System (BioRad, Hercules, CA). The purities of PAP were confirmed by SDS-PAGE.

The denaturant-induced equilibrium unfolding studies of PAP were performed by incubating PAP proteins in 10 mM sodium phosphate buffer (pH6.5) including various concentration of GuHCl for 5 h at 20 °C. The concentrations of wild-type and mutant PAP were conventionally determined using the molar extinctions of Trp, Tyr, and Phe included in PAPs. The molar extinction coefficient of PAP at 280 nm, ε_{280}, was 29,000 $M^{-1}cm^{-1}$. If not specified, the sample concentration was adjusted OD=0.1 at 280 nm for the fluorescence spectroscopic measurement.

CD and Steady-State Fluorescence Spectra

CD spectrum of PAP was recorded on a J-720 spectropolarimeter (JASCO, Tokyo, Japan). The concentration of proteins adjusted to 0.1 mg/ml. CD cuvette with 10 mm of optical path was used for the measurement in far UV wavelength region.

The steady-state fluorescence spectrum and anisotropy were measured with HITACHI 3010 fluorescence spectrophotometer (Tokyo, Japan). The excitation/emission bandpath was 5 nm/5 nm. The fluorescence emission spectrum was strictly corrected against the detection and excitation systems. The undesired effects caused by stray and scattering were removed with subtraction method.

The measurement of steady state fluorescence anisotropy was based on Eq. 1.

$$r_s = \frac{I_{vv} - GI_{vh}}{I_{vv} + 2GI_{vh}} \tag{1}$$

I_{vv} and I_{vh} were the intensities of parallel and perpendicular component against the vertically polarized excitation, respectively. G was the grating factor. One Gran-Taylor polarizer was set vertical at the excitation side and the other polarizer vertical and horizontal at the emission side to measure I_{vv} and I_{vh}. G factor was decided by measuring the intensity ratio of I_{vv} to I_{vh} against the horizontal excitation.

Fluorescence Intensity and Anisotropy Decay

The fluorescence intensity and anisotropy decay were measured by a sub-pico second laser based time correlated single photon counting (TCSPC) system. The excitation pulse of 285 nm and 295 nm were separated from a combination of sub-pico second pulse laser (TSUNAMI, Spectra-Physics, Mountain View, CA) synchronously pumped by green laser (Millenia XsJ, Spectra-Physics) with second harmonic generator/pulse selector (model 3980, Spectra-Physics) and third harmonic generator (GWU, Spectra-Physics). The fluorescence photon pulses were detected by a multi-channel plate type photomultiplier (3809U-50, Hamamatsu Photonics, Shizuoka, Japan) and fed into the start channel of a time-to-amplitude converter (TAC457, Ortec, Oak Ridge, TN) after the amplification by GHz AMP (model9327, Ortec). The stop signal for the time-to-amplitude convertor was obtained by detecting and amplifying the excitation pulse by APD (C5658, Hamamatsu Photonics). The output signal from TAC was stored in 2,048 channels of a multi-channel analyzer (Maestro-32, Ortec). The channel width was 12.7 ps. The fluorescence decay function was given by linear combination of some exponentials as Eq. 2,

$$F(t) = \sum \alpha_i \ \exp \ (-t/\tau_i) \tag{2}$$

where τ_i and α_i was the fluorescence decay time of i-th component and the corresponding pre-exponential factor. The decay kinetics and parameters were decided by convolution-non-linear least square methods based on the Marquard algorism [15, 16]. Their adequacy was

judged by the inspection of the residuals and statistical parameters such as sigma value (σ) and serial variance ratio (SVR).

The fluorescence anisotropy decay kinetics were given by

$$r(t) = \sum \beta_i \ \exp(-t/\tau_i) \tag{3}$$

where ϕ_i and β_i were the rotational correlation time of i-th component and the corresponding to the amplitude, respectively. The decay parameters were decided by the global analysis of I_{vv} and I_{vh}, since the Eq. 3 are satisfied between the fluorescence intensity decay, $F(t)$, and anisotropy decay, $r(t)$.

$$I_{vv} = \frac{1}{3}F(t)[1 - r(t)], \quad I_{vh} = \tfrac{2}{3}F(t)[1 - 2r(t)] \tag{4}$$

The quality of the fitting was confirmed similarly with the fluoresecence intensity decay. The instrument and analyzing methods of TCSPC used here was reported in the previous paper in detail [17].

Results and Discussion

Steady-State Fluorescence and CD

The fluorescence spectra of W208F- and W237F-PAP were shown in Fig. 2. Trp237 in W208F-PAP and Trp208 in W237F-PAP showed maxima at 348 and 336 nm to suggest that they were surrounded by polar and non-polar circumstances in the folded state respectively. Although data were not shown, the fluorescence maximum intensity of wild type PAP which included both of these two Trps was found at 342 nm. Increasing in the concentration of GuHCl to 2.5 M, the fluorescence spectrum of W208F-PAP shifted to the blue side and intensity decreased to about 50 %. On the other hand, the fluorescence of W237F-PAP shifted to red side. The fluorescence spectra of both of two mutant PAPs showed maxima at 356 nm when equilibrated with 3.5 M GuHCl. The equilibrated unfolding profiles of PAP were given in Fig. 3 by measuring the fluorescence intensity, maximum wavelength and anisotropy. The fluorescence maximum wavelengths of Trp237 and Trp208 were not affected by GuHCl in the concentration range of 0–2 M. The fluorescence spectra of PAP started to shift to the red

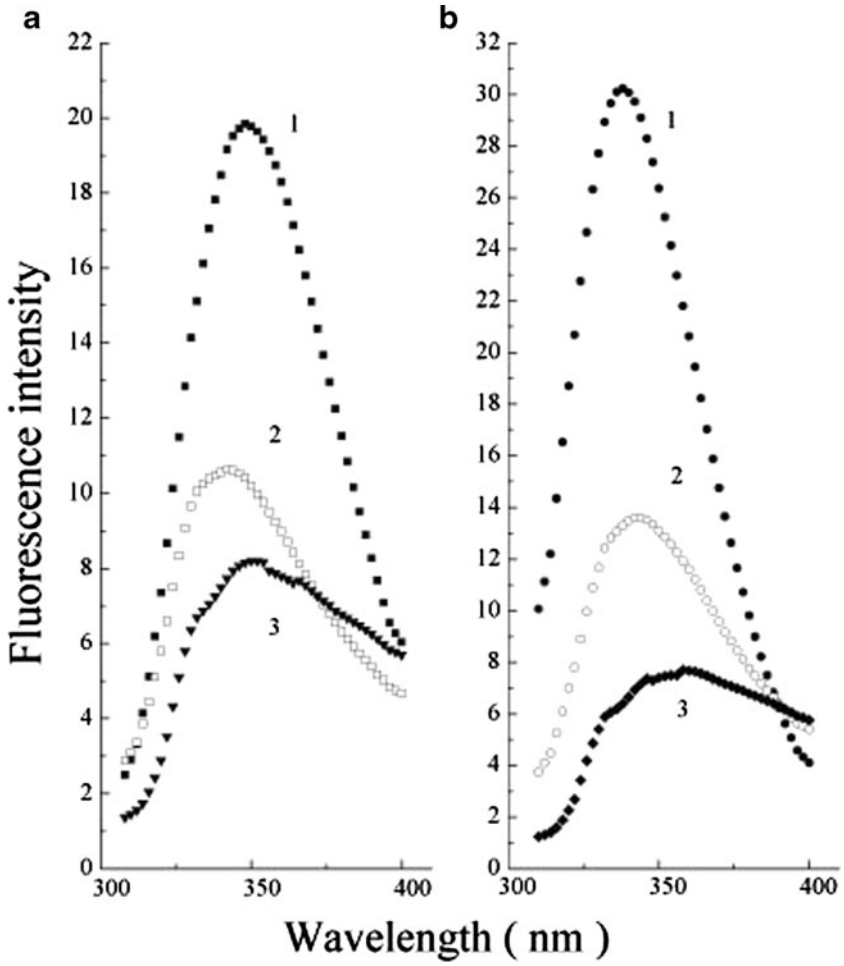

Fig. 2 Fluorescence Spectra of W208F-PAP (**a**) and W237F-PAP (**b**). The excitation wavelength was 295 nm. Curves 1, 2, and 3 in panel A and B were spectra measured after the incubation for 5 h in 10 mM phosphate buffer (pH6.5) including 0, 2.5, and 3.5 M of GuHCl, respectively. The sample concentrations were adjusted OD_{280}=0.1

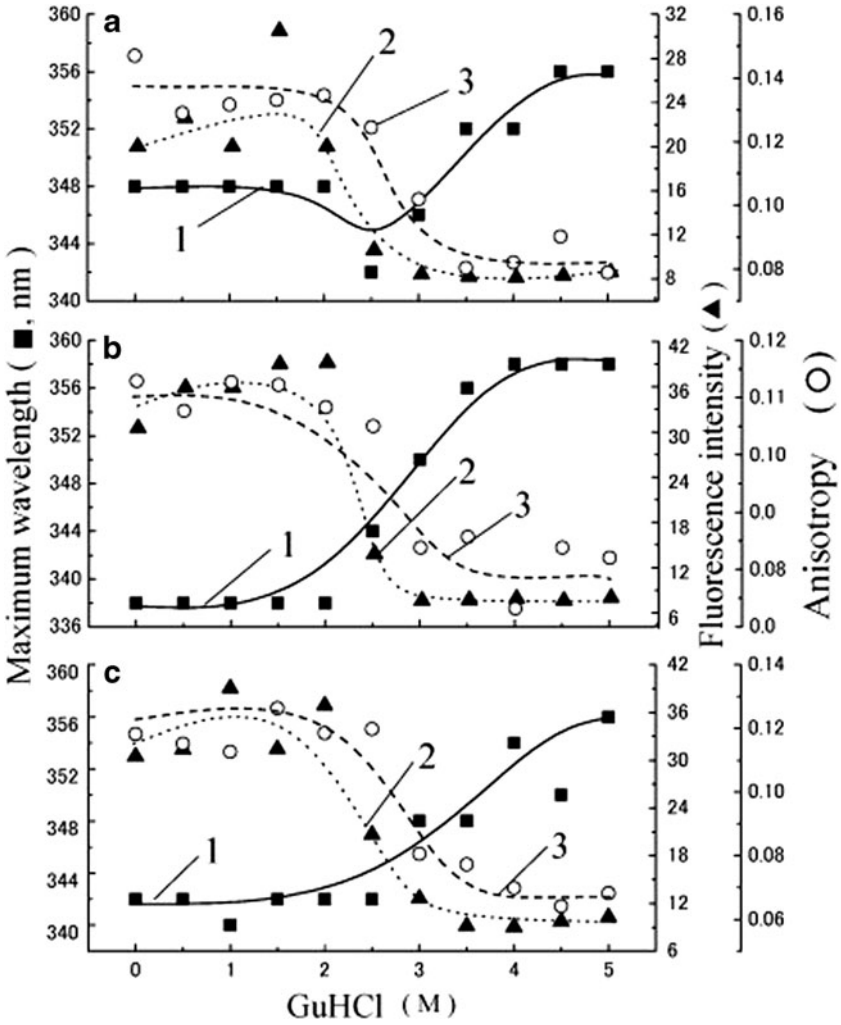

Fig. 3 The Unfolding Profiles of W208F-PAP (**a**) and W237F-PAP (**b**), and wild-type PAP (**c**). Curve 1 was monitored by the peak wavelength in the fluorescence spectrum. Curve 2 and 3 were fluorescence intensity and anisotropy, respectively. Every line was just for eye and not based on the analytical equation. The fluorescence intensity was the total emission from 300 to 400 nm. The fluorescence anisotropy was measured at 350 nm on the excitation at 295 nm. The sample concentration was adjusted OD_{280}=0.1. Every measurement was performed after incubation for 5 h

side at 2 M to reach to 355 nm at the presence of 3.5 M GuHCl. The fluorescence of mutant PAPs retained the higher intensity and anisotropy at 1–2 M of GuHCl. These results suggest that unfolding intermediate would intervene between the native and unfold state at the presence of 0–2 M of GuHCl.

CD spectra of PAPs at far UV regions and GuHCl concentration dependences of the secondary structure propensity were shown in Fig. 4. Any differences were not found in the line shapes of CD spectra of mutant and wild type PAPs. They showed large ellipticity at the wavelength of 210–225 nm in the folded state to suggest that the secondary structure of PAPs include almost even of α-helices and β-structures. The ellipticity at 222 nm of W237F-, W208F- and wild type PAP decreased below 1/5 with increasing in the concentration of GuHCl to 4 M. This result was consistent with one obtained by the fluorescence spectrum and anisotropy. The responses of CD spectra of mutant and wild-type PAPs were quite similar, but it should be noted that W208F-PAP showed smaller negative ellipticity than wild-type PAP at the folded state. This may be due to the destabilization of α-helix including Trp208 caused by the disappearance of hydrogen bond between indole ring of Trp208 and carbonyl moiety of Leu251. Correspondingly, the enzyme activity ratio, E_{W208F}/E_{WT} and E_{W237F}/E_{WT} which were estimated by measuring the liberated adenine from salmon sperm DNA were 0.62 and 0.90, respectively. These considerations and experimental results imply that Trp208 would participate in the stabilization of the local structure near the active site.

Energy Transfer Between Trp and Tyr

The fluorescence intensity decay curve of mutant PAP exhibited truncated form on the excitation at 285 nm in the folded state as shown in Fig. 5. On the other hand, the similar decay profile was not found by the excitation at 295 nm (data not shown). Such excitation wavelength dependence of the fluorescence decay of tryptophan residue is caused by the resonance excitation energy transfer from tyrosine to tryptophan residue. On the excitation at 285 nm, both of tyrosine and tryptophan residue are simultaneously excited, while tryptophan residue is exclusively

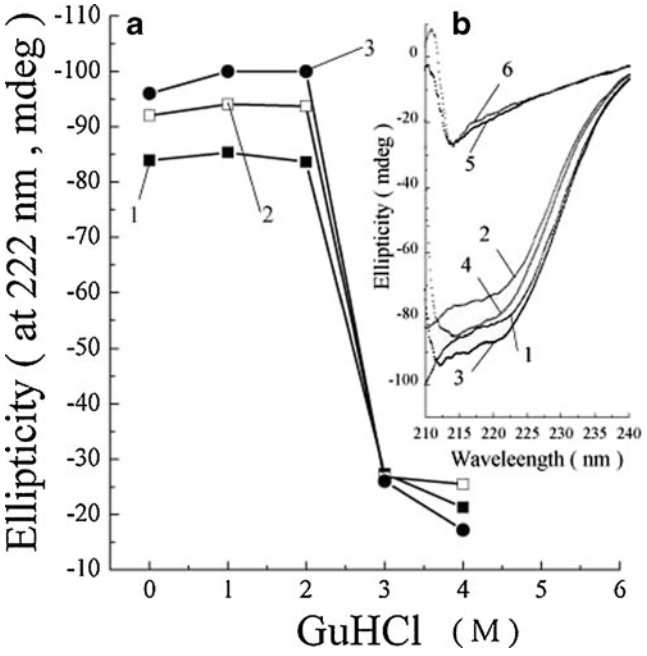

Fig. 4 The GuHCl Concentration Dependence of Ellipticity of Mutant PAPs. The ellipticity was monitored at 222 nm. Curve 1, W208F-PAP; curve 2, W237F-PAP; curve 3, wild-type PAP. PAP was equilibrated with 20 mM phosphate buffer including 0, 1, 2, 3, and 4 M GuHCl. The concentration of PAPs were adjusted to 3 μM/L (≈0.1 mg/ml). Insert, CD spectrum of W237F-PAP (curves 1, 3, and 5) and W208F-PAP (curves 2, 4, and 6). Curves 1 and 2, 0 M GuHCl; curves 3 and 4, 1 M GuHCl; curves 5 and 6, 3 M GuHCl

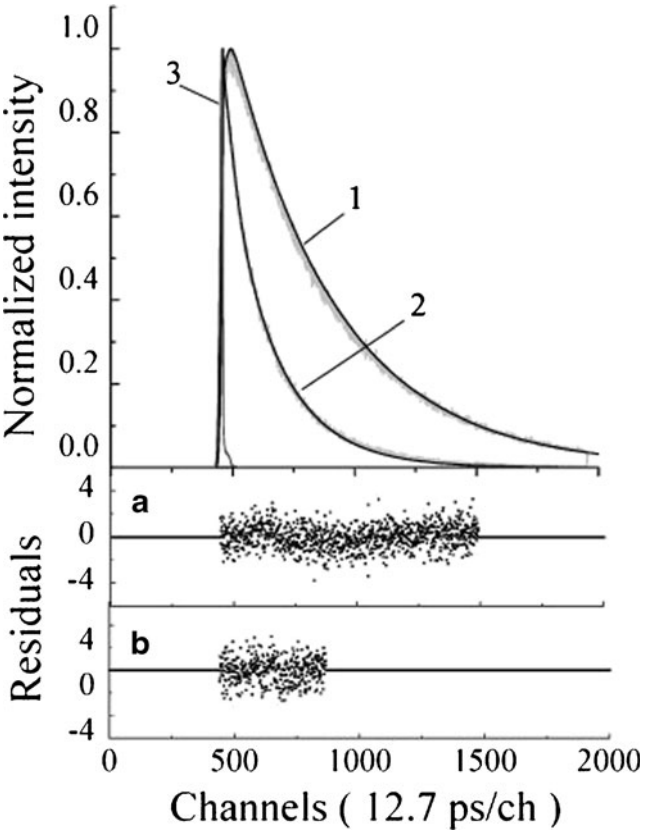

Fig. 5 The Fluorescence Intensity Decay Profiles of W237F-PAP. The excitation wavelength, 285 nm; emission wavelength, 360 nm. Curve 1, 0 M GuHCl; curve 2, 3 M GuHCl; curve 3, instrumental response function (IRF). The concentration of W237F-PAP was adjusted OD_{280} =0.1. The measurements were performed after incubation for 5 h. Experimentally measured curves were shown by thin lines. The *thick lines* were obtained by the decay parameters, α_i and τ_i, giving the best fits. The residual plots at 0 M and 3 M were shown in the lower panel of A and B, respectively

excited to the excited singlet state at 295 nm. Simple kinetic analysis demonstrates that the fluorescence decay of tryptophan residue is described with Eq. 5 when the energy transfer participates in the electronic relaxation of tryptophan residue.

$$F(t) = \frac{k_{et}D_0}{\left(\frac{1}{\tau_A}-\frac{1}{\tau_D}\right)}\left\{\exp\left(-\frac{t}{\tau_D}\right)-\exp\left(-\frac{t}{\tau_A}\right)\right\} + A_0\exp\left(-\frac{t}{\tau_A}\right) \quad (5)$$

where τ_A and τ_D are fluorescence lifetimes of the energy acceptor and donor, respectively, k_{et} the energy transfer rate constant and D_0 and A_0 are constants relating to the absorption of the donor and acceptor. Equation 5 indicates that the fluorescence decay parameters of tryptophan residue would give the negative pre-exponential factor and, therefore the decay profile with truncated form. Fluorescence decay parameters of W208F- and W237F-PAP were summarized in Table 1. The negative pre-exponential factors in the fluorescence decay kinetics of W237F-PAP were recognized at the concentrations of GuHCl lower than 2 M. Then, the decay time corresponding to the negative pre-exponential factor became longer with increasing in GuHCl. At the concentrations of GuHCl higher than 2 M, the decay profile steeply decayed and did not show negative pre-exponential factor. The negative pre-exponential factor of fluorescence decay of W208F-PAP was not observed

Table 1 Fluorescence decay parameter of mutant PAP on excitation at 285 nm

GuHCl	α_1	α_2	α_3	τ_1(ns)	τ_2(ns)	τ_3(ns)	σ	SVR
W208F-PAP								
0 M	1.18	0.05	−0.23	6.39	1.45	0.13	1.01	1.91
1 M	0.98	0.07	−0.05	6.29	2.19	0.22	1.00	1.99
1.5 M	0.94	0.06	–	6.13	1.75	–	1.04	1.93
W237F-PAP								
0 M	1.15	−0.15	–	5.57	0.16	–	1.02	1.91
1.5 M	1.08	−0.87	–	5.61	0.46	–	1.02	1.88
2 M	1.12	−0.11	–	5.63	0.54	–	1.03	1.88
3 M	0.10	0.04	0.86	2.62	0.53	0.04	0.99	1.97

Table 2 Energy transfer rate constant and distance between Trp and nearest neighboring Tyr

GuHCl	k_{et} (ns^{-1})	R (Å)
W208F-PAP (Trp237-Tyr182)		
0 M	8.02	8.2
1 M	4.23	9.1
W237F-PAP (Trp208-Tyr72)		
0 M	6.36	8.5
1.5 M	1.73	10.5
2 M	0.98	11.7

at the concentrations of GuHCl higher than 1.5 M. Since it is known that the fluorescence lifetime of tyrosine residue (τ_D) are 3.27 ns and the critical distance (R_0) for the energy transfer from Tyr to Trp is 14.0 Å [18-20], the energy transfer rate(k_{et}) and distance(R) of W237F- and W208F-PAP were estimated using Eq. 6.

$$k_{et} = \frac{1}{\tau_D}\left(\frac{R_0}{R}\right)^6 \tag{6}$$

The results were shown in Table 2. The energy transfer distance between Trp208 and the nearest neighboring Tyr was expanded 8.5 Å to 11.7 Å by the relaxation of the C-terminal domain adjacent to the N-terminal domain. W208F-PAP maintained the Trp-Tyr distance 8.2 Å in the folded state. But it increased to 9.1 Å equilibrated with 1 M GuHCl. When GuHCl concentration was increased higher, the negative pre-exponential factors were not found in the fluorescence decay of W208F-PAP. This suggests the energy transfer pair was disorganized. Probably, the energy transfer pair would be separated apart more than 28 Å

Table 3 Fluorescence anisotropy decay parameters of W237F-PAP and W208F-PAP. The rotational freedom f was estimated by $f = \frac{\beta_2}{\beta_1+\beta_2}$. The estimation of semi-cone angle for the rotation was based on Eq. 9

GuHCl	β_1	β_2	ϕ_1 (ns)	ϕ_2 (ns)	f	θ
W208F-PAP						
0 M	0.37	–	25.96	–	0	0
1 M	0.39	–	25.29	–	0	0
2.5 M	0.32	–	13.05	–	0	0
4 M	0.31	0.04	6.18	0.01	0.89	58°
W237F-PAP						
0 M	0.30	–	18.61	–	0	0
1 M	0.30	–	25.51	–	0	0
2 M	0.11	0.24	25.71	0.03	0.68	48°
4 M	0.09	0.27	7.61	0.06	0.75	49°

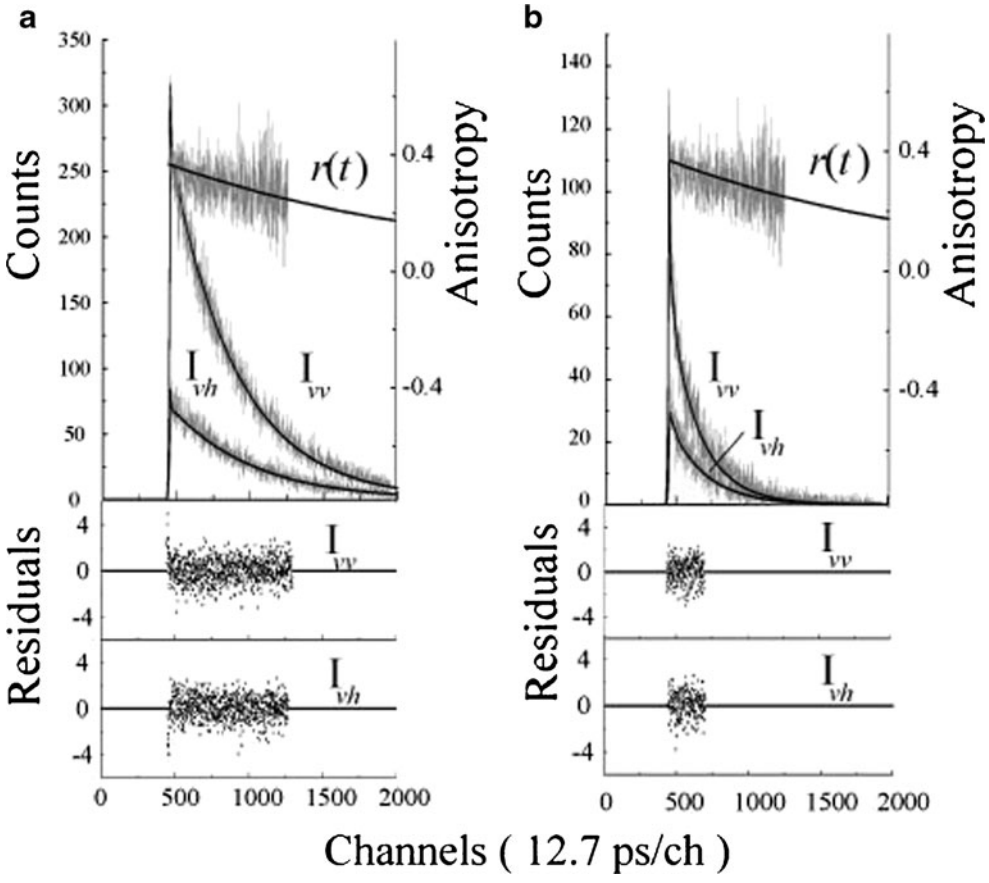

Fig. 6 The Fluorescence Anisotropy Decay of W237F-PAP. Panel A, 0 M GuHCl; Panel B, 4 M GuHCl. Excitation wavelength, 295 nm; emission wavelength, 360 nm. The decay curves experimentally measured were indicated by thin lines. The *thick lines* was fitting curves drowned by the decay parameters giving the best fits against the curve fitting to Eqs. 4 and 5 in text. The best-fit parameters were shown in Table 3. Anisotropy, the fluorescence anisotropy decay; I_{vv} and I_{vh}, the decay of the vertically and horizontally polarized fluorescence components against the vertical excitation, respectively. The residual plots for I_{vv} and I_{vh} were shown in the lower panel. The curve fitting was performed in the range of 0.1 $I_{vv(vh)}{}^{max}$ (rise) to 0.1 $I_{vv(vh)}{}^{max}$ (decay)

because the rate of energy transfer is much smaller when the energy transfer distance is extended two times longer than the critical distance.

Trp208 and Trp237 are arranged in the C-terminal domain and these two Trps are adjacent to N-terminal domain. According to the X-ray crystallographic structure of PAP, Trp237 locates 9.52 Å apart from Tyr182 and the distance between Trp208 and the closest Tyr72 is 7.94 Å [21]. These Trp-Tyr distances would be almost consistent with the distances estimated by the analysis of the energy transfer. The separation of these energy transfer pair suggests that unfolding of the tertiary structure of PAP was initiated with the separation of C-terminal domain from N-terminal domain at 1 M GuHCl and propagated to the active site adjacent to N-terminal domain at 2 M.

Time-Resolved Fluorescence Anisotropy

The fluorescence anisotropy decay of tryptophan residue in protein was generally described with linear combination of exponentials characterized with the rotational correlation time, ϕ_i, and the corresponding amplitude, β_i, as Eq. 3. The fluorescence anisotropy decay kinetics of two mutant PAPs were described with single or double exponential function according to the concentrations of GuHCl as shown in Fig. 6 and Table 3. The rotational correlation times observed here almost corresponded to the segmental and entire rotations of the tryptophan residue and PAP itself, respectively. Assuming the rotational motions of protein and Trp are independent, the fluorescence anisotropy decay, $r(t)$ is described with the Eq. 7 using the rotational correlation times, ϕ_f and ϕ_p corresponding to the rotations of Trp and protein, respectively [22].

$$r(t) = r_0\left[fe^{-\frac{t}{\phi_f}} + (1-f)\right]e^{-\frac{t}{\phi_p}} \tag{7}$$

Then, the decay parameters, ϕ_p, ϕ_f and f were related with the experimentally decided decay parameters as Eq. 8.

$$\phi_1 = \phi_p, \quad 1/\phi_2 = 1/\phi_p + 1/\phi_f, \quad f = \beta_2/(\beta_1+\beta_2) \tag{8}$$

Trp208 in W237F-PAP exhibited no motional freedom at the GuHCl concentrations below 2 M. At the presence of 2 M, the decay kinetics of W237F-PAP switched to double exponential function. This suggests that the local structure near the active site surrounding Trp208 would be relaxed. The rotational correlation time of Trp208 was about 30 ps and the freedom of the segmental rotation was 0.68. Further increasing of GuHCl concentration where PAP was unfolded, the rotational freedom was increased to 0.75. The longer correlation time was shortened to 7.61 ns by the unfolding of the total globular structure of PAP. The segmental rotation of Trp was depicted by semi-cone angle (θ) using the motional freedom [23, 24].

$$\sqrt{1-f} = \frac{1}{2}\cos\theta(\cos\theta + 1) \tag{9}$$

Trp208 would fluctuation rotate from −48° to 48° in the peptide matrix just before reaching to the unfold state.

The internal motion of Trp237 in W208W-PAPwas suppressed until PAP reach to the unfolded state since the fluorescence anisotropy decay was described with single exponential function. The rotational freedom of Trp237 was 0.89 and the semi-cone angle describing the rotation was in the range of ±58° in the unfold state.

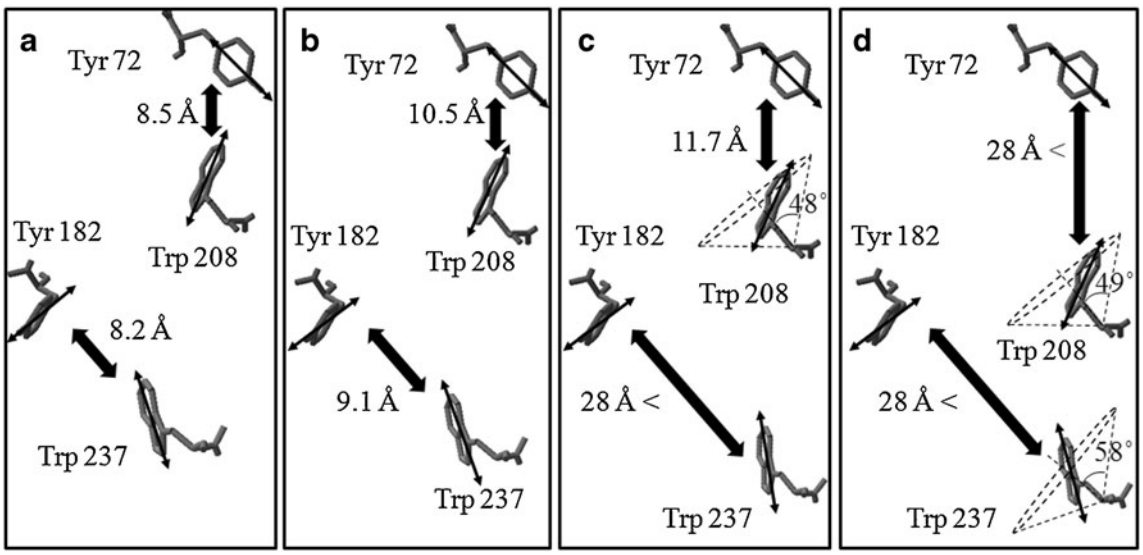

Fig. 7 The local structural changes around Trp208 and Trp237 under the GuHCl-induced unfolding of PAP. *Thin arrows* in the figure indicate the transition moment. The *broken lines* indicate the cone angles for the segmental rotations of Trp208 and Trp237. A, 0 M GuHCl; B, 1 M; C, 2 M; D, 4 M

Conclusion

In the denaturant-induced equilibrium unfolding study, the steady state fluorescence and CD spectra consistently demonstrated that PAP unfolded equilibrated with 4 M GuHCl. The specific deformation of tertiary structure were induced at the adjacent sites of the C-terminal and N-terminal domain before reaching to the unfold state. The local structural change near Trp208 and 237 by increase in GuHCl concentration were schematically represented in Fig. 7. The energy transfer pair between Trp237 and Tyr182 was disorganized to suggest that N-terminal domain would move away from C-terminal domain at 2 M of GuHCl. Even after the energy transfer pair was lost, the local structure surrounding Trp237 was compactly folded in the C-terminal domain. The other energy transfer pair between Trp208 and Tyr72 which located near active center was maintained until GuHCl was increased to 2 M, although the local structure near Trp208 was loose. Unfortunately, the GuHCl effect on the structure of N-terminal domain could not be described in the present study because there is no adequate fluorescence reporter available.

Momorcharins showed compactly folded unfolding intermediate in the unfolding process. 3D structure of PAP gradually became loose with increase in the denaturant and characteristic structural feature as the unfolding intermediate was found just preceding to the unfolding in spite of the structural similarity and high homology in the amino acid sequence.

References

1. Royer CA (2006) Probing protein folding and conformational transition with fluorescence. Chem Rev 106:1769–1784
2. Santra MK, Banerjee A, Krishnakumar SS, Rahaman O, Panda D (2004) Multiple-probe analysis of folding and unfolding pathways of human serum albumin: evidence for a framework mechanism of folding. Eur J Biochem 271:1789–1797
3. Ferguson N, Day R, Johnson CM, Allen MD, Daggett V, Fersht AR (2005) Simulation and experiment at high temperatures: ultrafast folding of a thermophilic protein by nucleation-condensation. J Mol Biol 347:855–870
4. Vendruscolo M, Paci E, Dobson CM, Karplus M (2001) Three key residues form a critical contact network in a protein folding transition state. Nature 409:641–645
5. Au TK, Collins RA, Lam TL, Ng TB, Fong WP, Wan DCC (2000) The plant ribosome inactivating proteins luffin and saporin are potent inhibitors of HIV-1 integrase. FEBS Lett 471:169–172
6. Wang Y-X, Jacob J, Wingfield PT, Palmer I, Stahl SJ, Kaufman JD, Huang PL, Huang PL, Lee-Huang S, Torchia DA (2000) Anti-HIV and anti-tumor protein MAP30, a 30 kDa single-strand type-I RIP, shares similar secondary structure and β-sheet topology with the A chain of ricin, a type-II RIP. Protein Sci 9:138–144
7. Corrado G, Bovi PD, Ciliento R, Gaudio L, Maro AD, Aceto S, Lorito M, Rao R (2005) Inducible expression of a *Phytolacca heterotepala* ribosome-inactivating protein leads to enhanced resistance against major fungal pathogens in tobacco. Phytopathology 95:206–215
8. Park S-W, Stevens NM, Vivanco JM (2002) Enzymatic specificity of three ribosome-inactivating proteins against fungal ribosomes, and correlation with antifungal activity. Planta 216:227–234
9. Endo Y, Mitsui K, Mochizuki M, Tsurugi K (1987) The mechanism of action of ricin and related toxic lectins on eukaryotic ribosomes. The site and the characteristics of the modification in 28 S ribosomal RNA caused by the toxins. J Biol Chem 262: 5908–5912
10. Fukunaga Y, Nishimoto E, Otosu T, Murakami Y, Yamashita S (2008) The unfolding of α-momorcharin proceeds through the compact folded intermediate. J Biochem 144:457–466
11. Fukunaga Y, Nishimoto E, Yamashita K, Otosu T, Yamashita S (2007) The partially unfolded state of β-momorcharin characterized with steady-state and time-resolved fluorescence studies. J Biochem 141:9–18
12. Honjo E, Watanabe K (1999) Expression of mature pokeweed antiviral protein with or without C-terminal extrapeptide in *Escherichia coli* as a fusion with maltose-binding protein. Biosci Biotechnol Biochem 63:1291–1294
13. Iizasa E, Nagano Y (2006) Highly efficient yeast-based in vivo DNA cloning of multiple DNA fragments and the simultaneous construction of yeast/*Escherichia coli* shuttle vectors. Biotechniques 40:79–83
14. Marykwas DL, Passmore SE (1995) Mapping by multifragment cloning in vivo. Proc Natl Acad Sci USA 92:11701–11705
15. Willis KJ, Szabo AG (1989) Resolution of tyrosyl and tryptophyl fluorescence emission from subtilisins. Biochemistry 28: 4902–4908
16. Zuker M, Szabo AG, Bramall L, Krajcarski DT, Selinger B (1985) Delta function convolution method (DFCM) for fluorescence decay experiments. Rev Sci Instrum 56:14–22
17. Otosu T, Nishimoto E, Yamashita S (2009) Fluorescence decay characteristics of indole compounds revealed by time-resolved area-normalized emission spectroscopy. J Phys Chem A 113:2847–2853
18. Lakowicz JR, Laczko G, Gryczynski I (1987) Picosecond resolution of tyrosine fluorescence and anisotropy decays by 2-GHz frequency-domain fluorometry. Biochemistry 26:82–90
19. Eisinger J, Feuer B, Lamola AA (1969) Intramolecular singlet excitation transfer. Applications to polypeptides. Biochemistry 8:3908–3915
20. Oishi O, Yamashita S, Nishimoto E, Lee S, Sugihara G, Ohno M (1997) Conformations and orientations of aromatic amino acid residues of tachyplesin I in phospholipid membranes. Biochemistry 36:4352–4359
21. Monzingo AF, Collins EJ, Ernst SR, Irvin JD, Robertus JD (1993) The 2.5 Å structure of pokeweed antiviral protein. J Mol Biol 233:705–715
22. Lakowicz JR (2006) Advanced anisotropy concepts. In: Principles of fluorescence spectroscopy, 3rd edn. Springer, New York, pp 413–441
23. Lipari G, Szabo A (1982) Model-free approach to the interpretation of nuclear magnetic resonance relaxation in macromolecules. 2. Analysis of experimental results. J Am Chem Soc 104:4559–4570
24. Nishimoto E, Yamashita S, Szabo AG, Imoto T (1998) Internal motion of lysozyme studied by time-resolved fluorescence depolarization of tryptophan residues. Biochemistry 37:5599–5607